PNAS
www.pnas.org

Supplementary Information for

Curling of epithelial monolayers reveals coupling between active bending and tissue tension

Jonathan Fouchard, Tom P.J. Wyatt, Amsha Proag, Ana Lisica, Nargess Khalilgharibi, Pierre Recho, Magali Suzanne, Alexandre Kabla, and Guillaume Charras

Corresponding authors : Alexandre Kabla, Guillaume Charras.
E-mail: ajk61@cam.ac.uk, g.charras@ucl.ac.uk

This PDF file includes:

Supplementary text
Figs. S1 to S6
Tables S1 to S2
Captions for Movies S1 to S13
References for SI reference citations

Other supplementary materials for this manuscript include the following:

Movies S1 to S13

Supporting Information Text

Supplementary methods

Fly stock. Flies were grown using standard culture techniques. A Sqh-TagRFPt[9B] knock-in line was used for imaging of Myosin II homolog in *Drosophila* during peripodial epithelium retraction (1). A Flytrap line Vkg-GFP[G0454] was used for imaging the dynamics of the collagen (extra-cellular matrix) during leg eversion (2). The Armadillo-GFP line is from Bloomington (number 8556).

Leg disc preparation. Leg discs were dissected from white pupae + 2 hours after puparium formation in Schneider's insect medium (Sigma-Aldrich) supplemented with 15% fetal calf serum, 0.5% penicillin-streptomycin and 2 µg/ml 20-hydroxyecdysone (Sigma-Aldrich, H5142). Leg discs were transferred onto a glass slide in 13.5 µL of this medium and confined between a 120 µm-deep double-sided adhesive spacer (Secure-Seal from Sigma-Aldrich) and a glass coverslip placed on top of the spacer. Halocarbon oil was added to the sides of the spacer to prevent evaporation. To visualize cell shapes during peripodial epithelium retraction, cell membranes were labeled after dissection and before imaging via a 10-minute incubation with Far red CellMask plasma membrane stain according to manufacturer instructions (Thermo Fisher Scientific). To prevent collagen remains from interfering with peripodial epithelium curling, a collagenase treatment (0.18 units/ml) was applied for 10 minutes simultaneously with CellMask incubation.

Confocal imaging of peripodial epithelium. Retraction and curling of peripodial epithelia were imaged at 24°C on an inverted confocal laser scanning microscope (LSM-880, Zeiss) equipped with an Airyscan detector and a 40X objective (C-Apochromat, NA=1.2, Zeiss). Images were acquired at a rate of one z-stack every 2-5min and z-slices were spaced by 0.5µm. Airyscan images were then reconstructed using the Airyscan processing module of the Zen Black software (Zeiss). Movies of the retraction were then generated using Imaris (Bitplane).

MDCK cell lines. MDCK-E-Cadherin-GFP cell lines (generated as described in (3)) were cultured in presence of 250ng/ml puromycin in the culture medium. MDCK NMHCIIA-GFP and MDCK NMHCIIB-GFP were generated as described in (4). Cells were then cultured in presence of G418 (1mg/ml) in the culture medium.

Imaging and quantification of Myosin II-GFP distribution in MDCK epithelia and Sqh-RFP distribution in *Drosophila* peripodial epithelia. To quantify the anisotropy of Myosin II along the apico-basal axis of suspended MDCK cells, z-stacks of MDCK monolayers expressing NMHCIIA–GFP or NMHCIIB–GFP were acquired using a high numerical aperture silicon oil 40X objective (UPLSAPO S, NA=1.25, Olympus) mounted on an Olympus IX83 inverted microscope equipped with a scanning laser confocal head (Olympus FV1200). Apical, medial and basal surfaces were segmented from images of the plasma membrane stained with Far red CellMask (Thermo Fisher Scientific). A z-projection of 2 focal planes separated by 1µm was generated at each position (apical, medial, or basal) to compensate for the slight tilt of the cells along the z-axis. Myosin II average intensity was then measured within the segmented regions. To account for background fluorescence, the average intensity of a focal plane above the apical zone was subtracted from the measurement. We also noticed the existence of a gradient of intensity along the thickness axis in the images of the plasma membrane stain. Such gradient was consistent with a decay of the incident and emitted light in the deeper regions of the cells. We thus took this effect into account in our calculation of the average intensity in the basal compartment as follows: $I_c^{bas} = (I^{bas} - I^n)\frac{I_m^{ap}}{I_m^{bas}}$ and $I_c^{ap} = I^{ap} - I^n$, where I_c^{ap} and I_c^{bas} are the corrected intensities of apical and basal Myosin II respectively, I^n is the intensity of the background (noise), I^{ap} and I^{bas} are the measured Myosin II intensities in the apical and basal domains respectively, and I_m^{ap} and I_m^{bas} are the intensities of the CellMask membrane marker in the apical and basal domains respectively.

Measurement of tissue curvature C and curled tissue length L_c. In this study, we always refer to tissue curvature to define out-of-plane tissue curvature. The curvature of MDCK monolayers or *Drosophila* peripodial epithelia along their contour length was determined as follows. First, the coordinates of the midpoint of each baso-lateral junction was manually determined from a profile view of the epithelium. A spline (*interpolate.splrep* of the *Scipy* Python library) was then fitted to these points to obtain the full monolayer profile. The local curvature κ along the monolayer contour length was subsequently computed every $1\mu m$ from the interpolating spline given parametrically (y(t), z(t)): $\kappa = \frac{|y''z' - y'z''|}{(z'^2+y'^2)^{\frac{3}{2}}}$. The spontaneous curvature of the tissue was defined as the average curvature within the tip region of the tissue (green region on Fig S1B). Note that the definition of monolayer tip is dependent on monolayer shape. Indeed, two categories of shapes could be identified based on tissue curvature. In some cases, the monolayer was only bent at the very edge (e.g. for Y27632 treated tissues), whereas in other cases the monolayer curled up on itself (see Fig 1F). The curled tissue length was defined in confocal profile views of the tissue from the last junction whose axis was perpendicular to the bulk tissue plane (xy plane, see Fig 3A) to the tip of the tissue. In the first case, the spontaneous curvature was defined within the entire length of curled tissue. In the latter case, the curvature was computed within the region after the y-coordinate of the tissue profile $y(l)$ starts to evolve non-monotonously with l.

The curled tissue length was defined from the last junction whose axis was perpendicular to the bulk tissue plane in confocal profile views of the tissue (see Fig 3A) to the tip of the tissue.

Mechanical manipulation of MDCK epithelial tissues for measurements of bending forces. Local unfolding of MDCK curled monolayers were performed as follows. A glass capillary was pulled with a micropipette puller (Narishige) and its tip was cut and glued to a second stiff glass capillary which was previously bent to accommodate the geometry of the setup. The stiffness k of the device was calibrated by pressing it against a Nitinol wire of known stiffness (see (3)) in order to serve as a force cantilever. Before the experiment, the force cantilever was approached in the vicinity of the curled tissue free edge of the MDCK monolayer. To unfold the tissue, a ramp of displacement $D(t)$ was imposed at the base of the device at a rate of 0.5 $\mu m.s^{-1}$ through a motorized platform (M-126.DG1 controlled through a C-863 controller, Physik Instrumente, via a Labview program). The displacement of the tip of the cantilever $\Delta(t)$ was then measured from confocal images after segmentation through the *Triangle* thresholding algorithm available in Fiji (5). The force required to unfurl the MDCK monolayer was then equal to: $F(t) = k.(D(t) - \Delta(t)) = k.\delta(t)$ with $\delta(t)$ the deflection of the cantilever.

Mechanical manipulation of MDCK epithelial tissues in the tissue plane: stretching and compression. Tissue-scale mechanical deformations in the plane of MDCK monolayers along the x-axis were applied as described in (6). Briefly, a custom-made adaptor was wedged in the top end of the hinged arm of the stretching device. The adaptor was connected to a 2-D manual micromanipulator mounted on a motorized platform (M-126.DG1 controlled through a C-863 controller, Physik Instrumente). Then, the tissues were deformed by moving the motorized platform via a custom-made Labview program (National Instruments). To image the same yz-profile of the tissue during stretching, that portion of the tissue needs to stay immobile in the microscope reference frame. For that, the motorized platform was interfaced with the microscope stage (PS3J100, Prior Scientific Instruments) through a custom-made Labview program as follows. If the tissue of length L_0 (i.e the initial distance between coverslips) was stretched by a length l and a profile located at a distance $x < L_0$ from the static coverslip was imaged, the stage was then moved by $-\frac{lx}{L_0}$ to compensate for the change in length of the tissue. The profile chosen in our experiments was the one where the deflection of the tissue was maximum, corresponding to $x \simeq \frac{L_0}{2}$.

Confocal imaging of MDCK epithelial tissues during mechanical manipulation. Tissues were imaged at 37°C in a humidified atmosphere with 5% CO2. The imaging medium consisted of DMEM without phenol red supplemented with 10% FBS. Profile views of the curled tissues during mechanical manipulation were obtained using a high numerical aperture silicon oil 30X objective (UPLSAPO S, NA=1.05, Olympus) mounted on an Olympus IX83 inverted microscope equipped with a scanning laser confocal head (Olympus FV1200). Each image consisted in roughly 100 slices spaced by $1\mu m$. Time series were acquired with an interval of $\simeq$1s. To visualize the tip of the cantilever, AlexaFluor-647-conjugated dextran (10,000 MW, Thermo Fisher Scientific, added at $20\mu g.ml^{-1}$) was added to the medium. In addition to staining the medium, we noticed that dextran accumulated at the cantilever tip, allowing for easy segmentation. While we do not know the cause of this accumulation, we hypothesize that it is due to preferential binding to the oxidized region of the pulled capillary.

Laser ablation of MDCK epithelial tissues. Laser ablation and subsequent imaging of MDCK tissues was carried out with a LSM880 scanning laser confocal system mounted on an inverted Axio Observer microscope stand (Zeiss). Ablation was performed through an infrared Ti:Sapphire laser tuned at 980nm (200 mW emission) over the thickness of the sample in rectangular regions (150 x 15 μm^2, 16 x 2 cells) situated in the centre of suspended MDCK monolayers. Confocal stacks were acquired through a 40X objective by exciting the fluorophores at the appropriate wavelength (LD C-Apochromat, NA=1.1, Zeiss). Each stack consisted in roughly 50 slices spaced by $1\mu m$. Time series were acquired every 20-60 seconds for 12 minutes minimum.

Statistics and data analysis. All data and statistical analysis were performed using the Python language environment and its scientific libraries (NumPy (7), SciPy (8)). Graphs were plotted using the Python library Matplotlib (9). Basic image processing was carried out with the Fiji package (5). All code is available from the corresponding author upon reasonnable request. The statistical significance between the different samples was assessed using the Mann-Whitney U test. Significance symbols were defined as follows: (****, p<0.0001), (***, p<0.001), (**, p<0.01), (*, p<0.05). All boxplots show the mean value (square), the median value (central bar), the first and third quartile (bounding box) and the range (whiskers) of the distribution.

Appendix 1 : Method to estimate the bending modulus of epithelial monolayers

We have designed a method to measure the force necessary to unfurl a curled suspended MDCK epithelial monolayer (Fig 3). Here, we describe how to calculate the 2-dimensional bending modulus B of such a tissue from these measurements, using an energetic method.

As the force cantilever is displaced along the y-axis perpendicular to the tissue free edge, it 1) unfurls the previously curled tissue and 2) stretches part of the flat tissue in the bulk. The work W_f performed by the cantilever along its displacement is then equal to the sum of the mechanical energies deforming the monolayer: W_c the bending energy necessary to change the curvature of the curled tissue from C_0 to C_1, and W_s the stretching energy of the bulk:

$$W_f = W_c + W_s \quad [1]$$

- Since the force in the cantilever grows linearly with the displacement of its tip (see Fig 3D), the work of the cantilever deforming the tissue, corresponding to a force F_1 and a course Δ_c of its tip ($\Delta_c = D - \delta$ in the main manuscript) is:

$$W_f = \frac{1}{2} F_1 \Delta_c \quad [2]$$

- The bending energy stored in tissue curling is:

$$W_c = \frac{1}{2} B L_c w_c ((C_1 - C_s)^2 - (C_0 - C_s)^2) \quad [3]$$

where B is the bending modulus, L_c the length of curled tissue and w_c the width of the deflected tissue (along the Ox-axis). C_s is the spontaneous curvature of the tissue. C_0 and C_1 are the average out-of-plane curvature along the curled region before and after force application respectively (Fig 3F).

- The stretching energy of the bulk is :

$$W_s = \frac{1}{2} E w_c L_b (\frac{\delta_b}{L_b})^2 \simeq \frac{1}{2} E {\delta_b}^2 \quad [4]$$

where E is the 2-D elastic modulus of the tissue $E = E_{3D}.h$, with E_{3D} the Young's modulus of the tissue, h the monolayer thickness, δ_b the deflection of the bulk and L_b the length over which the bulk tissue is deflected.

- As a result, the bending modulus of the tissue takes the form:

$$B = \frac{(F_1 \Delta_c - E {\delta_b}^2)}{L_c w_c ((C_1 - C_s)^2 - (C_0 - C_s)^2)} \quad [5]$$

- Extraction of the values in Equation 5:

  - L_c and h were measured from confocal profile views of the tissue. For L_c, see details in Supplementary methods, Fig 3A & 3F.

  - w_c and δ_b were measured from overlaying z-projections of confocal stacks of the tissue before and after unfurling with the cantilever (see Fig S3D).

  - Δ_c was measured through automatic segmentation of confocal images (see Supplementary methods).

  - E_{3D} was extracted from the slope of the linear phase in uni-axial tissue force-extension tests (Fig S5B).

  - C_s was determined as described in Supplementary methods and Fig S1B & S1C.

  - The bending modulus was then calculated for each tissue tested. The average value was: $B = (1.9 \pm 0.3).10^{-13}$ N.m (N=9). Tables S1 and S2 provide the typical values of the parameters and quantities measured in this article.

Appendix 2 : Model of 2D elastic thin sheet to capture the coupling between in-plane and out-of-plane epithelial monolayer shape

Summary. We model here the epithelial monolayer as an elastic rectangular bi-dimensional sheet clamped to two infinitely rigid plates. Despite their active nature, we have demonstrated the elastic behaviour of MDCK monolayers at intermediate time-scales (30s to 15min): first, in-plane, their macroscopic response to stretch was elastic (6); second, out-of-plane, we could show in Fig S3C that stresses do not dissipate after unfurling of the tissue by a force cantilever. Moreover, the thin film approach is justified by the fact that the tissue thickness ($\simeq 10\mu m$) is about 2 orders of magnitudes lower than its other dimensions ($\simeq$ 1mm).

In the model, we decompose the internal mechanical energy into a stretching and a bending energy (10). To mimic the out-of-plane stresses of active origin, the sheet is endowed with a spontaneous curvature (11–14). The sheet is then characterized by its 2D bending modulus B, its 2-D stiffness E and its spontaneous curvature C_s. We do not consider here that activity may modify the functional form of the stretching and bending energies.

The ultimate shape of the tissue will be determined by a balance between curling - which relaxes the spontaneous curvature while deflecting the tissue inwards - and stretching of the free edge which varies according to the position of the plates and the amount of curled tissue. Our aim is to determine the maximum deflection of the tissue d caused by curling at the tissue free edge depending on monolayer boundary conditions.

Calculation of the deflection of the sheet. We start from a hypothetical initial configuration where a sheet of width w and length L_0, clamped on two of its sides, is fully flattened (Fig S6,(i)). The energy associated to this state corresponds to the energy required to cancel the spontaneous curvature C_s:

$$E_0 = \frac{1}{2} w L_0 B C_s^2 \quad [6]$$

We then assume the sheet to be free to curl, which will deflect the tissue inwards by a distance d (Fig S6, (ii)). Yet, due to the clamped sides of the sheet, the free edge of the tissue gets stretched. We approximate the free edge interface by two straight segments. (This is a simplification since the free edge of the monolayer possess an arc shape in our experiments.) The curled region of area $\frac{1}{2} d L_0$ now has a curvature C_s (second term in the equation below). We assume that this area is then stretched with a strain $\epsilon_c(d, L_0)$ corresponding to the extension of the free edge from a length L_0 to a length $2l$ (third term in the equation below, Fig S6, (ii)). The fourth term in the equation represents the stretching energy of the bulk (strain ϵ). The energy E_1 of the sheet can then be written as :

$$E_1(\epsilon, d) = E_0 - \frac{1}{2} d L_0 B C_s^2 + \frac{1}{2} d L_0 E \epsilon_c^2 + \frac{1}{2} L_0 E \epsilon^2 (w - d) \quad [7]$$

We can rewrite ϵ_c as a function of l (where $2l$ is the new length of the free edge) and L_0 :

$$\epsilon_c = \epsilon + \frac{2l}{L_0} - 1 = \epsilon + \sqrt{4(\frac{d}{L_0})^2 + 1} - 1 \quad [8]$$

We then search for d which minimizes E_1 (Fig S6, (iii)) :

$$\frac{\partial E_1(\epsilon, d)}{\partial d}|_\epsilon = 0 \quad [9]$$

We solved this equation numerically. It predicts the evolution of monolayer deflection d (corresponding to the curled tissue length) as a function of the sample's initial length L_0 and the deformation ϵ through only three parameters: the 2-D stiffness E, the bending modulus B and the spontaneous curvature C_s. Importantly, all these parameters could be measured in our setup. Fig S5C shows that the model prediction is in agreement with the variations of deflection measured without any fitting parameter.

Also, setting $\epsilon = 0$ in this equation predicts how the deflection evolves with the sample's initial length L_0. We find that d is proportional to L_0: $d = \alpha L_0$, which we could observe experimentally with the fitting pre-factor $\alpha_{exp} = 0.50$ (Fig 5F). This value is higher than the pre-factor predicted by the model $\alpha_{th} = 0.27$. This difference could be due to the fact that 1) the collagen substrate takes also the form of an arc shape at its edge (see Fig 1A) and 2) the deflection of the collagen substrate also grows with the distance between cover-slips.

Table S1. Typical quantities measured during unfurling experiments of MDCK suspended monolayer

Quantity	Symbol	Value ± Std Dev	unit
Monolayer thickness	h	15.1±1.1	µm
Cantilever diameter	d_c	9.0±3.7	µm
Cantilever force	$F_1 - F_0$	58±48	nN
Curvature before unfurling	C_0	$(4.8\pm3.3).10^4$	m^{-1}
Curvature after unfurling	C_1	$(2.2\pm1.3).10^4$	m^{-1}
Curled length	L_c	50±22	µm
Width of deflected tissue	w_c	68±14	µm
Bulk tissue extension	δ_b	2.9±2.0	µm
Cantilever tip displacement	Δ_c	20±7	µm

Table S2. Measured material properties - MDCK suspended monolayer

Parameters	Symbol	Value ± Std Err	unit
3D Young's modulus	E_{3D}	940±98	Pa
2D elastic modulus	E	(1.4±0.2).10^{-2}	Pa.m
Bending modulus	B	(1.9±0.3).10^{-13}	N.m
Spontaneous curvature	C_s	(7.9±0.7).10^{4}	m^{-1}

Figure S1

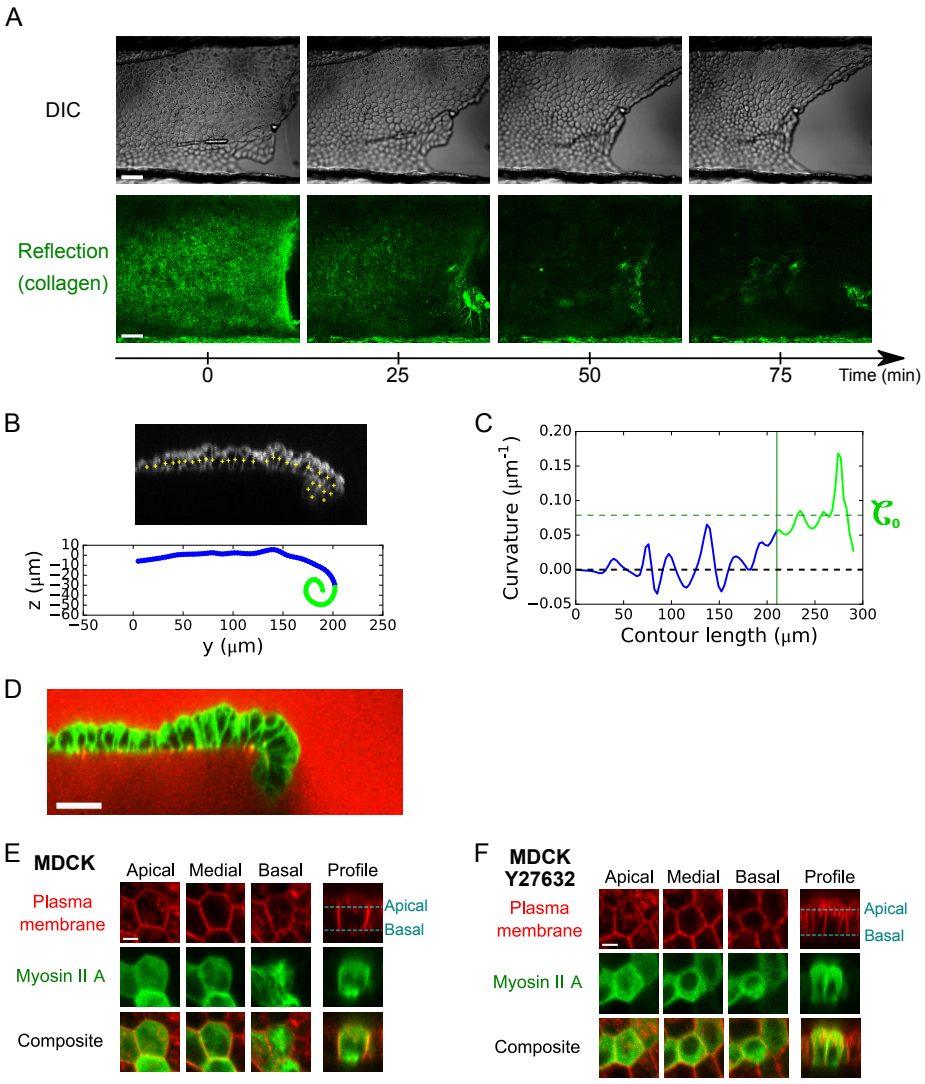

Fig. S1. (A) Time-series showing the shape changes of the free edge of an MDCK monolayer during the digestion of the collagen substrate with collagenase (N=14). Top: DIC imaging shows changes of tissue shape. Bottom: Confocal reflection microscopy imaging shows the dynamics of collagen digestion. Scale bars: 50μm. (B) Extraction of the monolayer profile contour. Top: Profile view of an MDCK monolayer obtained through confocal scanning laser imaging. Cell membranes are marked with CellMask. The coordinates of the midpoint of each baso-lateral junction are manually positioned (yellow crosses). Bottom: A spline is fitted to these coordinates to define the monolayer contour. (C) The local curvature is calculated along the monolayer contour length in 1μm steps. The spontaneous curvature of the tissue is determined as the average curvature within the tip region of the tissue free edge (green part in B and C, see Supplementary methods). In this example, the tip is defined as the region after the y-coordinate of the tissue profile y(l), where l is the contour length of the tissue, evolved non-monotonously with l (see green region in B, bottom). (D) Scanning laser confocal image showing the profile view (yz-plane) of a representative suspended MDCK monolayer. Cell membranes are marked with CellMask (green). The medium is marked with Dextran-Alexa647 (red). Note that no medium can be observed inside the curl, indicative of a very high curvature of the monolayer. (E) Localisation of Myosin II A-GFP in the apical, medial and basal regions of a substrate-free MDCK monolayer. Plasma membrane is marked with CellMask. Scale bar: 5μm. (F) Localisation of Myosin II A-GFP in the apical, medial and basal regions of a substrate-free MDCK monolayer treated with 25μM Y27632. Plasma membrane is marked with CellMask. Scale bar: 5μm.

Figure S2

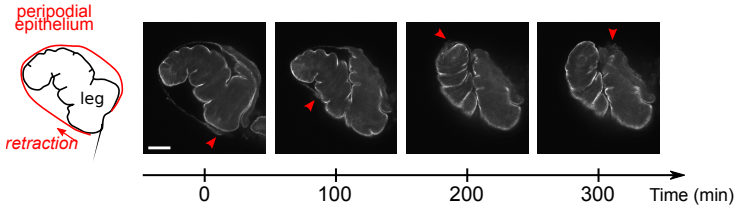

Fig. S2. Low magnification confocal imaging of a *Drosophila* leg undergoing eversion. The outer peripodial epithelium (in red on the diagram) retracts, while the leg epithelium (center) changes shape. Red arrowheads indicate the retracting peripodial epithelium. Cell junctions are marked with Armadillo-GFP (*Drosophila* homolog of β-catenin). Scale bar: 50μm.

Figure S3

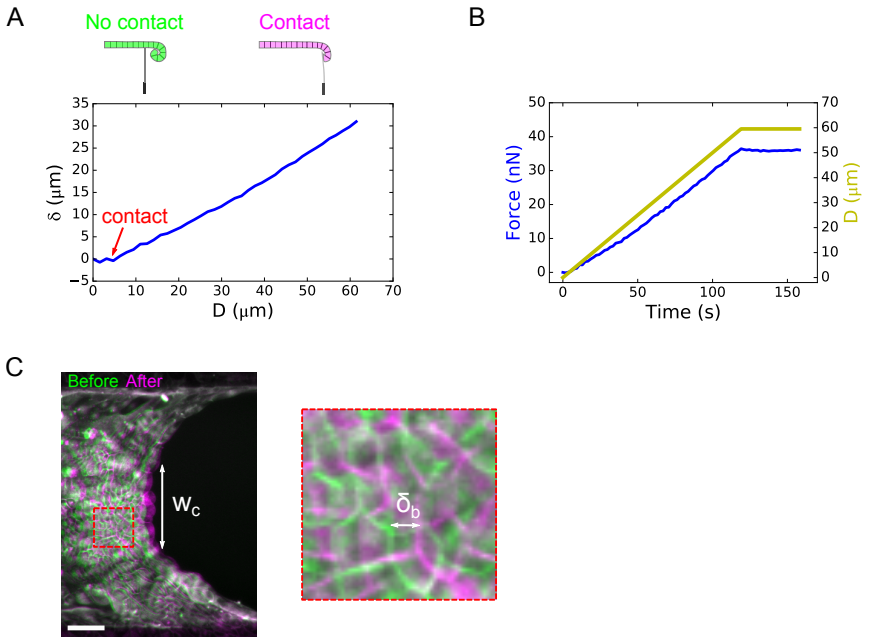

Fig. S3. (A) Deflection δ of the cantilever during unfurling of a suspended MDCK monolayer as a function of the displacement D imposed at its base by the motorized stage. The deflection is zero before contact with the tissue (see diagram above). The red arrow shows the contact point between the cantilever and the tissue. When the cantilever comes into contact with the curled tissue and unfurls it, the restoring force of the tissue results in a cantilever deflection. (B) Representative graph of the temporal evolution of force (blue) in response to a ramp of displacement (yellow) imposed at the cantilever base. Only negligible force change is observed after the movement is stopped, indicating that out-of-plane forces have an elastic origin and that a bending modulus of the tissue can be extracted from these measurements. (C) Overlay of scanning laser confocal images of the free edge of an MDCK monolayer (z-projection) before (green) and after (magenta) unfolding of the tissue with the force cantilever. w_c shows the width of deflected tissue. The zoomed region (right) shows the displacement of cell outlines in the bulk of the monolayer, here noted δ_b. Cell membranes are marked with CellMask. Scale bar: 50μm.

Figure S4

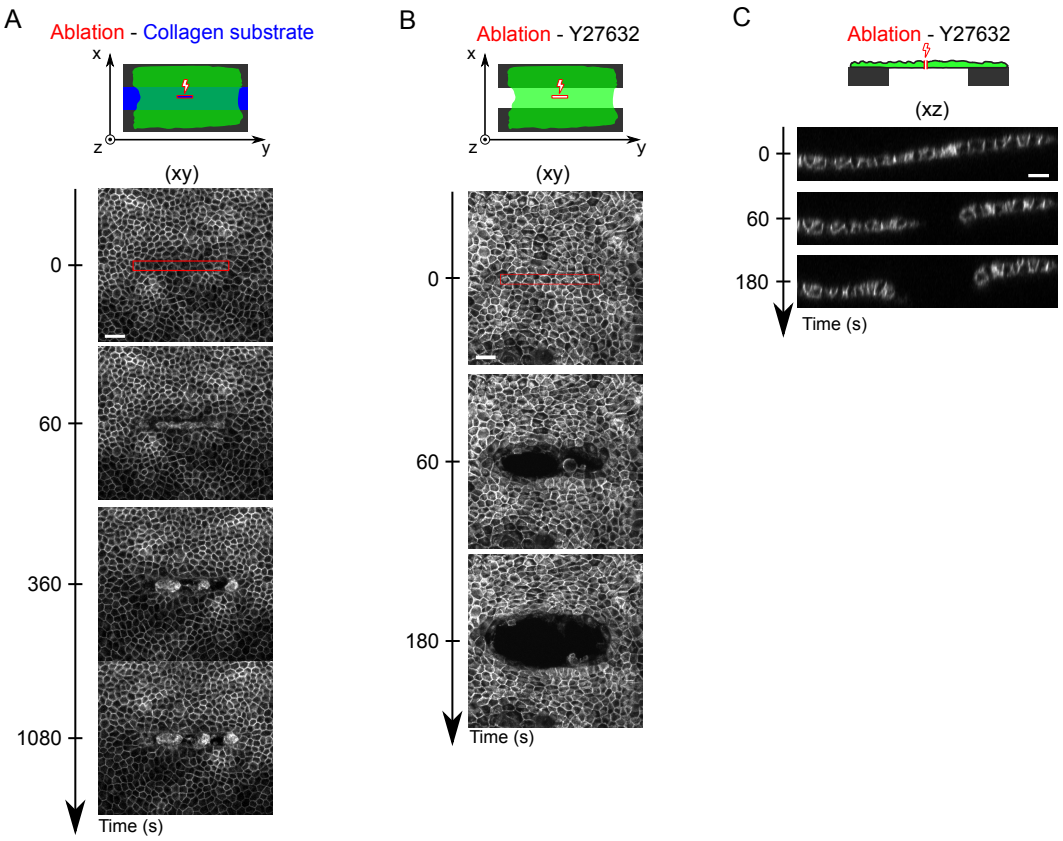

Fig. S4. (A) Time series of ablation of an MDCK monolayer (green on the diagram) adhering to a collagen substrate (blue) (N=6). The red rectangle indicates the ablated region. Laser ablation was performed after t=0s. Cell junctions are marked with E-Cadherin-GFP. Scale bar: 30μm. (B) Time series of the ablation of a suspended MDCK monolayer treated with 25μM Y27632, representative of N=10 monolayers. Laser ablation was performed in the frame after t=0s. Cell junctions are marked with E-Cadherin-GFP. Scale bar: 30μm. (C) Time-lapse profile view (xz-plane) of a suspended MDCK monolayer treated with 25μM Y27632 before (t=0s) and after laser ablation. Cell junctions are marked with E-Cadherin-GFP. Scale bar: 20μm.

Figure S5

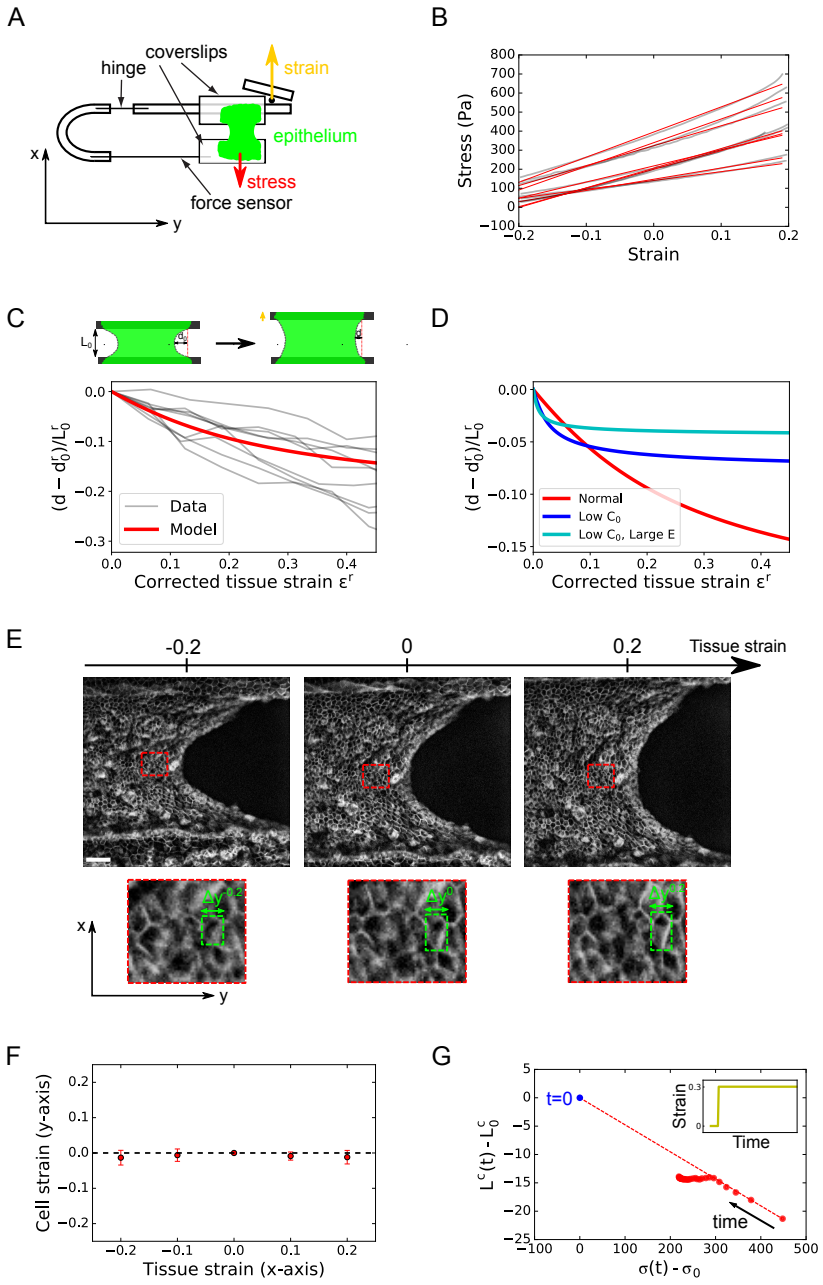

Fig. S5. (A) Diagram showing the setup for application of uni-axial tissue-scale strain and for stress measurement in suspended epithelia. (B) Tissue stress as a function of strain for N=8 individual samples (curves liatha). Red lines indicate the linear fit whose slope defines the Young's modulus of each tissue E_{3D}. (C) Variation of tissue deflection $d - d_0$ normalized by monolayer rest length L_0^r as a function of in-plane corrected tissue strain $\epsilon^r = \frac{L - L_0^r}{L_0^r}$. d_0 is the deflection at null strain. Here, tissue strain is corrected to have L_0^r as the rest length of the epithelium. L_0^r is defined experimentally as the deformation at which the tissue buckles under compression (see (6)). It is inferior to L_0, which corresponds to the gap between coverslips after collagen digestion. The grey lines represent each experimental dataset, the red line represents the response predicted by the model with the average parameters measured in MDCK monolayers and no free parameters (see main manuscript and Appendix 2). (D) Same as A for the response predicted by the model with different parameters. The response with the average parameters measured in MDCK cells is shown in red (as in B). The response with reduced spontaneous curvature $\frac{1}{10} C_s^{MDCK}$ is shown in blue. The response with reduced spontaneous curvature and increased elastic modulus $10 E^{MDCK}$ is shown in cyan. (E) Top: Confocal images of the free edge of a suspended MDCK monolayer for -20%, 0%, 20% tissue strain. Cell junctions are marked with E-Cadherin-GFP. Bottom: zoom on a region illustrating the negligible cell shape changes along the y-axis as cells are stretched and compressed along the x-axis (Δy defines the width of the cell bounding box). Scale: 50µm. (F) Cell strain along the y-axis $\frac{\Delta y^{\epsilon} - \Delta y^0}{\Delta y^0}$ as a function of tissue stretch along the x-axis. Cells analyzed are chosen within the first five rows next to the curled region and close to where the monolayer edge is tangent to the x-axis (N=20 cells from 4 different monolayers, data points represent the mean ± SE). (G) Average variation of curled length as a function of average variation of stress before and after a fast step of stretch. The red dashed line links the time-points just before and just after the step is applied. Note the alignment with part of the stress relaxation phase.

Figure S6

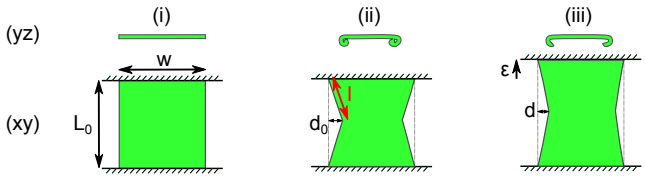

Fig. S6. Schematic diagram showing the configurations of the elastic model used to determine the deflection of the monolayer free edge as a function of tissue in-plane strain. The monolayer is modeled as a rectangular sheet of length L_0 and width w clamped on two of its sides. (i) Flattened configuration. (ii) Curled configuration. The free edge of length $2l$ is stretched and the monolayer curls giving rise to a deflection of the free edge, whose maximum is d_0 (iii) Curled and stretched configuration. The deflection of the free edge d decreases in response to stretching (strain ϵ).

Movie S1. Time-lapse of the free edge of an MDCK monolayer during the digestion of its collagen substrate by collagenase. Left: DIC imaging of the monolayer. Right: Collagen matrix imaged by confocal reflection microscopy. Collagenase is introduced in the medium at time t=0 min. Time is in min:sec. Scale bar: 50μm.

Movie S2. Time-lapse of the profile view of an MDCK monolayer during the digestion of its collagen substrate by collagenase. Collagenase is introduced in the medium at time t=0 min. Cell membranes are marked with CellMask. Time is in min:sec. Scale bar: 30μm.

Movie S3. Time-lapse of a Drosophila leg undergoing eversion. The outer peripodial membrane cracks and retracts, while the leg epithelium (center) changes shape. The red arrowhead indicates the retraction front. Cell junctions are marked with Armadillo-GFP (*Drosophila* homolog of β-catenin). Time is in min:sec. Scale bar: 50μm.

Movie S4. Time-lapse of a retracting peripodial epithelium imaged through Airyscan confocal microscopy. Top: Three-dimensional reconstruction. Bottom: Profile view perpendicular to the retraction front. Cell membranes are marked with CellMask. Time is in min:sec. Scale bar : 20μm.

Movie S5. Time lapse of an MDCK monolayer being unfurled by a cantilever that is displaced along the y-axis (profile view in the yz-plane). The medium is marked via Dextran-Alexa647 (red). Note that this dye also stains the tip of the cantilever underneath the monolayer, which facilitates the measurement of its displacement. Cell membranes are marked with CellMask (green). Time is in min:sec. Scale bar: 20μm.

Movie S6. Time-lapse of an MDCK monolayer grown on a collagen substrate undergoing laser ablation and subsequent wound healing. The red rectangle defines the border of the ablated region. Cell junctions are marked with E-Cadherin-GFP. Time is in min:sec. Scale bar: 30μm.

Movie S7. Time-lapse of a suspended MDCK monolayer undergoing laser ablation. The red rectangle defines the border of the ablated region. Cell junctions are marked with E-Cadherin-GFP. Time is in min:sec. Scale bar: 30μm.

Movie S8. Time-lapse of the profile of a suspended MDCK monolayer undergoing laser ablation. The profile view was taken along the plane perpendicular to the longest axis of the cut. Cell junctions (green) are marked with E-Cadherin-GFP, the medium (red) is marked with Dextran-Alexa647. Time is in min:sec. Scale bar: 20μm.

Movie S9. Time-lapse of the profile of a suspended MDCK monolayer treated with 25μM Y-27632 undergoing laser ablation. The profile view was taken along the plane perpendicular to the longest axis of the cut. Cell junctions are marked with E-Cadherin-GFP. Time is in min:sec. Scale bar: 20μm.

Movie S10. Time-lapse of the profile of a suspended MDCK monolayer before and after cut along the full length of the tissue at the interface with the coverslip. The profile view is taken along the plane perpendicular to the cut. Time is in min:sec. Scale bar: 30μm.

Movie S11. Time-lapse of the profile view of the free edge of a suspended MDCK monolayer during a ramp of in-plane strain. The profile view was taken along the plane perpendicular to the stretch axis. The movie starts at 0% strain, the monolayer is subsequently stretched to 90% strain, then compressed to -30% strain and finally brought back to 0%. (Strain is defined with reference to the monolayer length after digestion of collagen.) Cell membranes are marked with Cell Mask. Time is in min:sec. Scale bar: 30μm.

Movie S12. Time-lapse of the free edge of a suspended MDCK monolayer during a ramp of in-plane strain . The movie starts at 0% strain, the monolayer is subsequently stretched to 30% strain, compressed to -30% and brought back to 0%. (Strain is defined with reference to the monolayer length after digestion of collagen.) Time is in min:sec. Scale bar: 50μm.

Movie S13. Time-lapse of the profile of the free edge of a suspended MDCK monolayer before and after a step of in-plane strain (30% stretch). The profile view along the plane perpendicular to the stretch axis. Cell junctions are marked with E-Cadherin-GFP. Time is in min:sec. Scale bar: 30μm.

References

1. A Proag, B Monier, M Suzanne, Physical and functional cell-matrix uncoupling in a developing tissue under tension. *Development* **146**, dev172577 (2019).
2. X Morin, R Daneman, M Zavortink, W Chia, A protein trap strategy to detect gfp-tagged proteins expressed from their endogenous loci in drosophila. *Proc. Natl. Acad. Sci.* **98**, 15050–15055 (2001).
3. AR Harris, et al., Characterizing the mechanics of cultured cell monolayers. *Proc. Natl. Acad. Sci.* **109**, 16449–16454 (2012).
4. N Khalilgharibi, et al., Stress relaxation in epithelial monolayers is controlled by the actomyosin cortex. *Nat. Phys.* **15**, 839–847 (2019).
5. J Schindelin, et al., Fiji: an open-source platform for biological-image analysis. *Nat. methods* **9**, 676 (2012).
6. TP Wyatt, et al., Actomyosin controls planarity and folding of epithelia in response to compression. *Nat. materials* **19**, 109–117 (2020).
7. S Van Der Walt, SC Colbert, G Varoquaux, The numpy array: a structure for efficient numerical computation. *Comput. Sci. & Eng.* **13**, 22 (2011).
8. E Jones, T Oliphant, P Peterson, , et al., Scipy: Open source scientific tools for python. (2001).
9. JD Hunter, Matplotlib: A 2d graphics environment. *Comput. science & engineering* **9**, 90 (2007).
10. Q Li, TJ Healey, Stability boundaries for wrinkling in highly stretched elastic sheets. *J. Mech. Phys. Solids* **97**, 260–274 (2016).
11. Y Klein, E Efrati, E Sharon, Shaping of elastic sheets by prescription of non-euclidean metrics. *Science* **315**, 1116–1120 (2007).
12. E Efrati, E Sharon, R Kupferman, Elastic theory of unconstrained non-euclidean plates. *J. Mech. Phys. Solids* **57**, 762–775 (2009).
13. J Dervaux, P Ciarletta, MB Amar, Morphogenesis of thin hyperelastic plates: a constitutive theory of biological growth in the föppl–von kármán limit. *J. Mech. Phys. Solids* **57**, 458–471 (2009).
14. M Pezzulla, N Stoop, X Jiang, DP Holmes, Curvature-driven morphing of non-euclidean shells. *Proc. Royal Soc. A: Math. Phys. Eng. Sci.* **473**, 20170087 (2017).